Quadruple H-bonding cross-linked supramolecular polymeric materials as substrates for stretchable, antitearing, and self-healable thin film electrodes

Yan, Xuzhou; Liu, Zhiyuan; Zhang, Qiuhong; Lopez, Jeffrey; Wang, Hui; Wu, Hung-Chin; Niu, Simiao; Yan, Hongping; Wang, Sihong; Lei, Ting; Li, Junheng; Qi, Dianpeng; Huang, Pingao; Huang, Jianping; Zhang, Yu; Wang, Yuanyuan; Li, Guanglin; Tok, Jeffery B.-H.; Chen, Xiaodong; ...Bao, Zhenan

2018

Yan, X., Liu, Z., Zhang, Q., Lopez, J., Wang, H., Wu, H.-C., . . . Bao, Z. (2018). Quadruple H-bonding cross-linked supramolecular polymeric materials as substrates for stretchable, antitearing, and self-healable thin film electrodes. Journal of the American Chemical Society, 140(15), 5280-5289. doi:10.1021/jacs.8b01682

https://hdl.handle.net/10356/137694

https://doi.org/10.1021/jacs.8b01682

Quadruple H-bonding Crosslinked Supramolecular Polymeric Materials as Substrates for Stretchable, Anti-Tearing, and Self-Healable Thin Film Electrodes

Xuzhou Yan[†,#], Zhiyuan Liu[‡,#], Qiuhong Zhang[†,§,#], Jeffrey Lopez[†], Hui Wang[‖,¶], Hung-Chin Wu[†], Simiao Niu[†], Hongping Yan[†], Sihong Wang[†], Ting Lei[†], Junheng Li[†], Dianpeng Qi[‡], Pingao Huang[‖,¶], Jianping Huang[‖], Yu Zhang[‖], Yuanyuan Wang[‖], Guanglin Li[‖], Jeffery B.-H. Tok[†], Xiaodong Chen[‡,*], and Zhenan Bao[†,*]

[†]Department of Chemical Engineering, Stanford University, Stanford, CA 94305, United States.

[‡]Innovative Center for Flexible Devices, School of Materials Science and Engineering, Nanyang Technological University, 50 Nanyang Avenue, Singapore 639798, Singapore

[§]Department of Polymer Science and Engineering, School of Chemistry and Chemical Engineering, Nanjing University, Nanjing 210093, P.R. China

[‖]CAS Key Lab of Human-Machine Intelligence-Synergy Systems, Shenzhen Institutes of Advanced Technology, Chinese Academy of Sciences (CAS), Shenzhen 518055, P. R. China

[¶]Shenzhen College of Advanced Technology, University of Chinese Academy of Sciences, Shenzhen 518055, P. R. China

ABSTRACT

Herein, we report a *de novo* chemical design of supramolecular polymer materials (SPMs **1**–**3**) by condensation polymerization, consisting of: (i) soft polymeric chains (polytetramethylene glycol and tetraethylene glycol), and (ii) strong and reversible quadruple H-bonding cross-linkers (from 0 to 30mol%). The former contributes to the formation of the soft domain of the SPMs and the latter furnishes the SPMs with desirable mechanical properties, thereby producing soft, stretchable, yet tough elastomers. The resulting SPM-**2** was observed to be highly stretchable (up to 17,000% strain), tough (fracture energy ~30,000 J/m^2), and self-healing, which are highly desirable properties and are superior to previously reported elastomers and tough hydrogels. Furthermore, gold thin-film electrode deposited on this SPM substrate retains its conductivity, and combines high stretchability (~400%), fracture/notch insensitivity, self-healing, and good interfacial adhesion with the gold film. Again, these properties are all highly complementary to commonly used polydimethylsiloxane-based thin film metal electrodes. Last, we proceed to demonstrate the practical utility of our fabricated electrode via both in-vivo and in-vitro measurements of electromyography (EMG) signals. These

fundamental understanding obtained from the investigation of these SPMs will facilitate the progress of intelligent soft materials and flexible electronics.

INTRODUCTION

Demands for wearable and implantable electronics have boosted the development of various advanced materials, smart devices, and engineering methodologies.[1–3] As such, skin-inspired mechanically compliant sensors and actuators have been extensively reported as well as their potential for applications in prosthetics,[4] brain/machine interfaces,[5] and soft robotics.[6] Stretchable electrodes with high toughness play a crucial role in integrating various devices together to support functions under large mechanical deformations.[2] During the last few years, a variety of structural designs, such as wrinkled,[7] serpentined,[8] meshed,[9,10] and micro-cracked,[11,12] have been used to reduce degradation of conductivity under mechanical strain. To date, stretchable thin film metal electrodes, particularly gold electrodes, are typically deposited on polydimethylsiloxane (PDMS) substrates. But they have several limitations, such as being sensitive to fracture/notch, poor interfacial adhesion, lack of self-healing ability, *etc*. Therefore, it is of interest to address these limitations in thin film stretchable gold electrodes.

Compared to self-healable composite electrodes (usually prepared by mixing a self-healing polymer matrix and a conductive material[13–15]), fabricating skin-inspired thin film gold electrodes which are stretchable, self-healing, fracture insensitive, with good interfacial adhesion, and with matched modulus between electrode and human tissue, is highly challenging.[16] Here, we hypothesize that crosslinking through supramolecular chemistry will help to address the above deficiencies because the crosslinkers are dynamic so that the supramolecular polymeric materials (SPMs) can be designed to possess both good mechanical strength and adaptability. Thus, this may be a promising direction for the design of desirable substrates for skin-inspired thin film gold electrodes.[17–21]

Suo and coworkers previously reported a highly stretchable (tensile strain ~2000%) and tough (fracture energy ~9000 J/m^2) supramolecular polymeric hydrogel by incorporating a combination of ionically and covalently cross-linked networks.[22] However, depositing gold film electrodes on a water-containing hydrogel substrate in a high vacuum chamber is not practical. Furthermore, water vapor may result in the risk of electrical shorting. Guan *et al* prepared a biomimetic supramolecular polymer using cyclic 2-ureido-4-pyrimidinone (UPy) cores as the repeating units, which showcased a rare combination of high strength, high toughness, self-healing, and shape memory.[23] However, its high Young's modulus (~200 MPa) and relatively low fracture onset strain (~100%) limits its use for skin-inspired stretchable substrates. Evidently, materials that meet a rigorous set of requirements associated with mechanical properties for skin-inspired thin film electrodes are rare.

Herein, we report the design and preparation of a series of supramolecular polymeric materials (SPMs) **0**–**3**, wherein various amounts of stronger quadruple H-bonding UPy and weaker urethane crosslinks are introduced into polymeric backbones to tune the mechanical properties of SPMs (Figure 1a). Based on their mechanical behaviors, SPM-**2** is chosen as the polymeric substrate since it combines medium tensile stress (0.91 MPa), high stretchability (~17,000%), high toughness (fracture energy ~30,000 J/m^2), human tissue-compatible Young's modulus (~375 KPa), and efficient autonomous self-healing ability. Subsequently, we develop a SPM-**2** supported high performance thin film gold electrode, which exhibits a high stretchability of ~400%. Even for the electrode containing a notch, a stretchability of ~250% was achieved, which could be useful for surgical and implantable medical applications. Unexpectedly, SPM-**2** also lends the self-healing ability on its supported stretchable thin film gold electrode. The self-healed electrode recovered its original conductivity and showed a healed stretchability of ~90%, which is comparable or even superior to previously reported composite self-healing electrodes. The interfacial adhesion between SPM-**2** and thin film gold was enhanced by six times compared to PDMS-supported thin film gold electrode. Finally, the superior electric and mechanical properties of the self-healing and stretchable gold electrode allow us to demonstrate its utility in detecting electromyography (EMG) on both skin and in vivo.

RESULTS AND DISCUSSION

Materials design and synthesis. Gold films usually were found to crack easily on most elastic materials.[24,25] Additionally, the lack of either anti-tearing feature or good adhesion is a big obstacle. To meet the requirements of skin-inspired film electrodes, i.e. stretchable, self-healing, and fracture toughness, we synthesized a series of supramolecular polymeric materials (SPMs **0**–**3**) with increasing densities of the strong quadruple H-bonding UPy units as crosslinkers from 0 to 10mol%, 20mol%, and 30mol% via condensation polymerization, in which a polytetramethylene glycol (PTMG, M_n = 1000 g/mol)-based prepolymer was first prepared in the presence of two equivalents of isophorone diisocyanate (IPDI) and catalytic amount of dibutyltin dilaurate (DBTDL), followed by chain extension using tetraethylene glycol (TEG) and 5-(2-hydroxyethyl)-6-methyl-2-aminouracil in a pre-set ratio (Scheme S1). Compared to methylenediphenyl 4,4'-diisocyanate (MDI) and hexamethylene diisocyanate (HDI), the combination of PTMG and the bulkier IPDI makes the resultant polymer soft which is a key parameter for utilization in skin-inspired film electrodes.

However, in view of the potential applications inside or in contact with organisms, it is necessary to make the polymeric materials with Young's modulus <500 KPa.[16] Therefore, we employ TEG as a chain extender, which also plays a role to make the polymeric backbone more flexible and less crystalline. To endow these polymers with good mechanical properties, non-covalent cross-linkers were designed to take advantage of strong hydrogen bonding. Specifically, the well-known quadruple hydrogen bonding 2-ureido-4-pyrimidinone (UPy) motif developed by Meijer and coworkers was chosen because it offers an appealing combination of high thermodynamic stability (ΔG = ~10 Kcal/mol; $k > 10^7$ M^{-1} in chloroform) and rapid kinetic reversibility (k_{off} = ~8 s^{-1}),[26,27] which are favorable parameters to furnish our new SPMs with satisfactory mechanical behaviors. Moreover, the presence of self-complementary UPy units was not expected to disrupt the PTMG-based soft domain, thus making SPMs soft, stretchable, self-healing, yet tough.

Materials characterizations. Proton nuclear magnetic resonance spectroscopy (^{1}H NMR) indicated the successful preparation of SPMs as indicated by the presence of characteristic peaks of IPDI, PTMG, and TEG segments in polymeric backbones (Figures S2, 4, 6, 8). For SPMs **1**–**3**, the N-H signals on UPy units showed large downfield shifts (observed between 10.0 and 13.0 ppm) and low intensities (Figures S4, 6, 8), giving evidence for UPy dimerization which is the driving force for the formation of cross-linked polymeric network.[28a] Furthermore, FTIR spectra and solid-state ^{1}H NMR were used to confirm the presence of the quadruple H-bonding in our prepared materials (Figure S8b and 10a). All polymers were obtained with comparable number-averaged molecular weights (M_n) in the range of 37 to 41 KDa and relatively narrow (≤1.48) polydispersity index (PDI, calculated by M_w/M_n) as measured by gel permeation chromatography (GPC) utilizing *N*, *N*-dimethylformamide (DMF) as the eluent and poly(methyl methacrylate) (PMMA) as the standard (Figure 1c). According to our obtained molecular weights, the average number of UPy units in the polymeric chains was calculated to be ~3.0, 5.0 and 7.0 for SPMs **1**–**3**, respectively. Also, differential scanning calorimetry (DSC) study conveyed that glass transition temperatures (T_gs) are indeed present in SPMs **0**–**3**. The T_gs are in the range of -47.6 to -43.3°C for the soft PTMG segments in the polymeric backbones (Figure S10), suggesting that the introduction of hard UPy cross-linkers in SPMs has no obvious influence on the T_g of soft domain, which is a requirement for low modulus yet tough elastomer. Small-angle X-ray scattering (SAXS) of bulk SPMs displayed broad scattering peaks, indicative of the presence of microphase separation on the order of 3.7 to 5.2 nm (Figure 1d). To gain more insights into bulk materials properties of SPMs, small amplitude oscillatory shear (SAOS)

experiments were carried out. In the master curves scaled by time temperature superposition (TTS), all SPMs have crossover frequencies (ω_c) between storage modulus (G') and loss modulus (G''), at which G' (ω_c) = G''(ω_c) (Figure 1e). At low frequency (ω), G'' is larger than G', showing that the viscous property of SPMs is dominant. Upon increasing frequency, G' goes up faster than G'' and the elastic property of SPMs is predominant at the region of $\omega > \omega_c$. Increasing the UPy amount of SPMs from 0 to 30% leads to higher rubber plateau and longer terminal relaxation time which is estimated as the reciprocal of ω_c. Accordingly, the crossover points of G' and G'' of SPMs move to lower frequency, which means the samples are more solid-like at lower frequency.

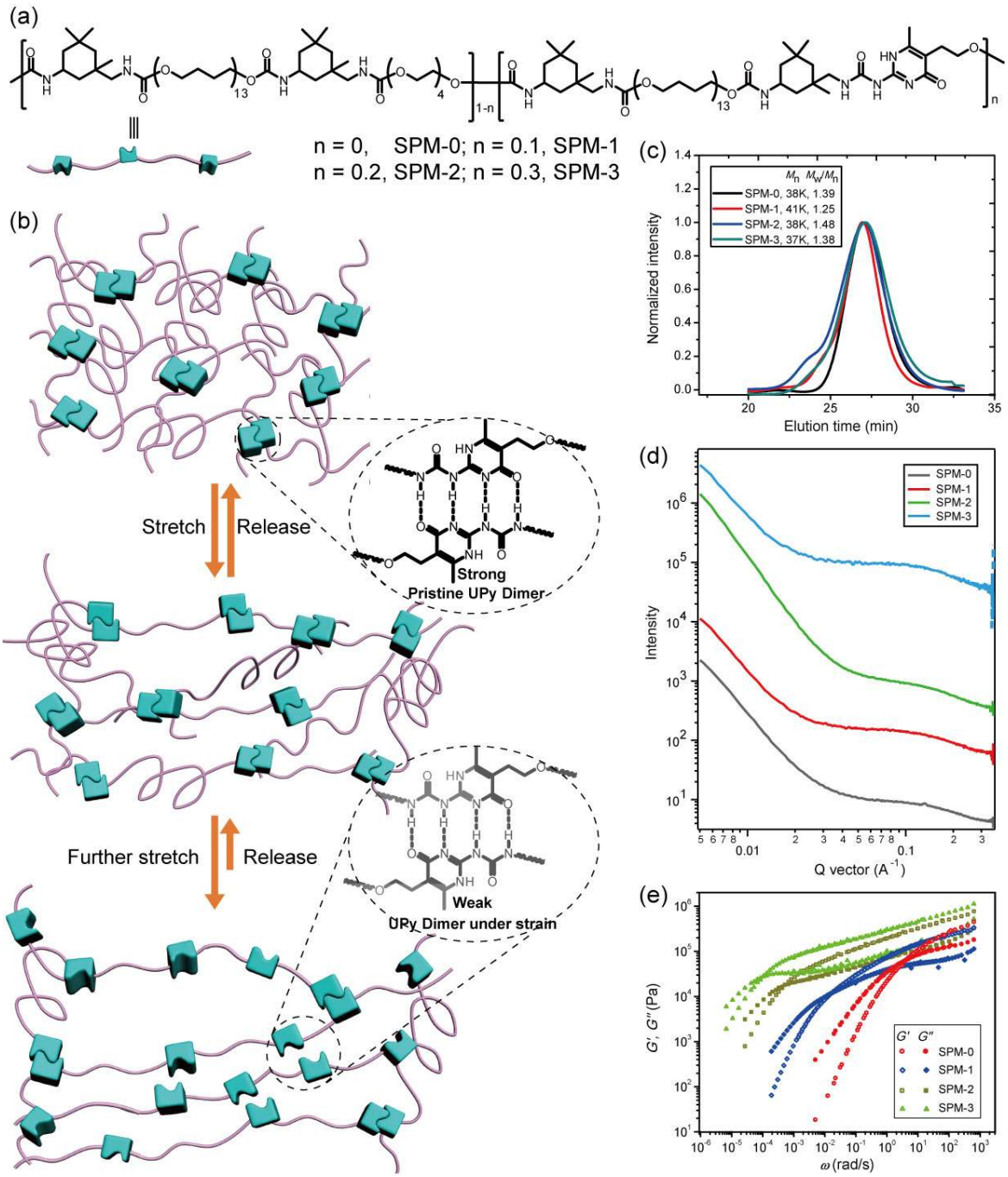

Figure 1. Schematic illustration of the design of stretchable supramolecular polymeric materials (SPMs) and general materials characterization. (a) Chemical structures of SPMs **0**–**3** with varying amounts of UPy cross-links to tune mechanical properties. (b) Cartoon representation of the proposed mechanism for highly stretchable SPMs. (c) GPC elution curves of SPMs **0**–**3** with DMF as the eluent and PMMA as the standard, showing that M_n and PDI of all polymers are comparable and relatively narrow, respectively. (d) SAXS profile plot for bulk SPMs which supports the presence of microphase separation on the order of 3.7 to 5.2 nm. (e) Master curves of SPMs shifted by time-temperature superposition (TTS). Frequency sweep of SPMs were performed from 100 to 20 °C with an interval of 20 °C over a span of three decades of frequency between 0.628 and 628 rad/s (reference temperature 20 °C, 1% strain).

Mechanical properties. The mechanical properties of SPMs **0**–**3** vary greatly depending on the different amounts of UPy crosslinks embedded in the polymeric backbones (Figure 2). As shown in Figure 2b, tensile stress-strain curves of SPMs suggest that an increase in UPy contents led to an improvement in mechanical performances, such as stretchability and tensile strength. SPM-**0**, i.e. without UPy crosslinks, displays weak mechanical strength, e.g. passing yielding point at 75% strain, it behaves as a viscoelastic fluid (Figure 2b). Upon increasing UPy units to 10 mol%, the mechanical behaviors such as tensile stress and strain of SPM-**1** improve a lot. However, due to insufficient crosslinkers, an obvious necking phenomenon was observed when it was stretched to 90× its original length (Figure 2b). A further increase of UPy amount to 20 mol% clearly enhances the maximum strain and stress respectively. It is worth mentioning that SPM-**2** also possesses remarkable mechanical strength so that it readily holds a weight 16,000× greater than its own without breaking (Figure S13). Finally, SPM-**3** with a 30 mol% UPy motif exhibits a maximum stress up to 3.74 MPa but markedly decreased stretchability of 3,100%. Therefore, overall SPM-**2** shows superior stretchability compared to most other self-healing polymers and tough hydrogels (Figure S14).[22,29–31] These observations indicate that the incorporation of various amounts of UPy crosslinking units is effective in systematically tuning mechanical properties. Similar observations have also been reported previously,[24,35b] in which both the strength and numbers of hydrogen bonds were observed to affect the mechanical properties of the resulting materials.

The high stretchability of our SPMs may originate from the crosslinking through the strong, highly directional quadruple H-bonding motif of UPy in the polymeric backbones. Previous work on metal-ligand crosslinked polymer, in which ligands were incorporated into the polymer backbone, showed high stretchability. It was attributed to the reversible formation of intramolecular loops within the same chain and intermolecular loops between different polymeric chains.[25] Similar conformation is possible here via the UPy dimerization. In the unstrained state, the intrachain loops result in the folding of the polymeric backbone which enables a considerable chain extension under deformation. Meanwhile, the interchain loops contribute to the formation of crosslinked polymeric network which further enhances the mechanical properties (Figure 1b). Due to the reversible nature of UPy moieties, the opening of intrachain or interchain loops by progressively disrupting the H-bonds upon stretching should bring about the unfolding and sliding of the polymeric networks, thereby enhancing the stretchability and toughness of SPMs. Moreover, due to the high bonding strength of UPy motif, we hypothesized that the UPy units may be only partially broken or have the chance to be close to other broken UPy units in adjacent chains, leading to dimerization and the

formation of a weak temporary cross-link under strain (Figure 1b). These peculiar binding and exchanging modes of quadruple UPy H-bonding along with abundant H-bonding-directed intra- and inter-chain loops in polymeric networks cooperatively lead to our observed high stretchability in SPMs.

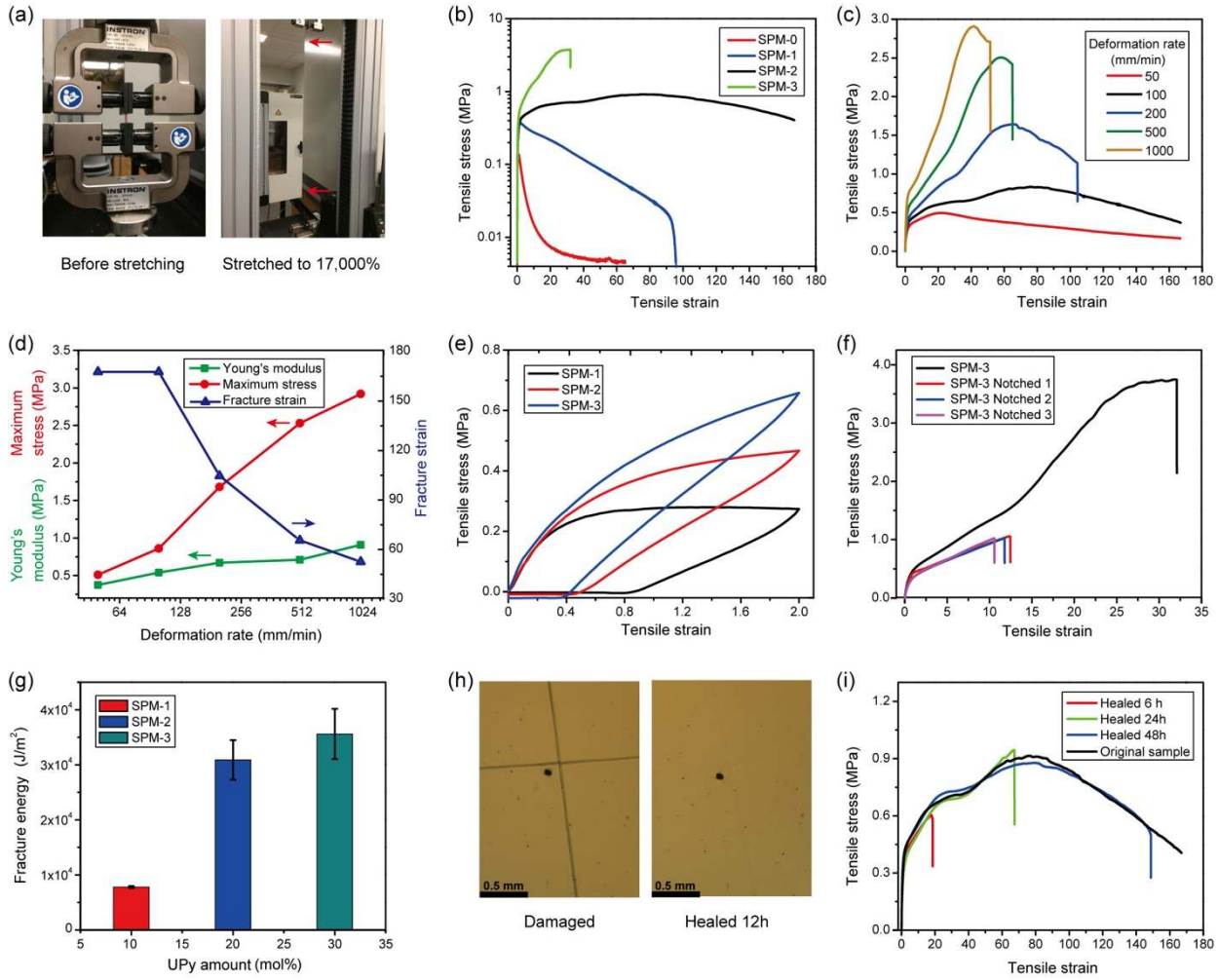

Figure 2. Mechanical properties of SPMs. (a) Photographs of a SPM-**2** test specimen before and after stretching to 17,000%. Red arrows show where is the stretched specimen. (b) Stress-strain curves of SPMs **0**–**3** with different cross-linking densities which have a pronounced impact on the mechanical properties. Maximum strain and stress reach 17,000% and 0.91 MPa for SPM-**2** with 20% UPy motif, respectively. Deformation rate: 100 mm/min. (c) Tensile behaviors of SPM-**2** under different deformation rates in the range of 50 to 1000 mm/min. (d) Deformation rate dependence of SPM-**2** on maximum stress, fracture strain, and Young's modulus. (e) Cyclic tensile tests of SPMs **1**–**3** at a strain of 200% under the deformation rate of 100 mm/min. The pronounced hysteresis accounts for the great energy dissipation ability of SPMs, a pivotal characteristic for high toughness. (f) Stress-strain curves of the unnotched and notched samples of SPM-**3**. A notch of 1 mm in length was made in the middle of a rectangular specimen of about 1 mm in thickness and 5 mm in width. The specimen was fixed in the two clamps with a pre-set distance of 10 mm. Deformation rate: 100 mm/min. (g) Fracture energy as a function of UPy amount of SPMs. The fracture energy of >30,000

J/m^2 is the highest value in the reported polymeric elastomers and tough hydrogels. (h) Optical microscope images of damaged and healed SPM-**2** film. (i) Stress–strain curves of the original and self-healed SPM-**2** specimens after three different healing times from 6 to 24 and then to 48h at room temperature. Deformation rate: 100 mm/min.

The stretching speed-dependent tensile behavior (Figure 2c) is consistent with the proposed chain dynamics as shown in Figure 1b. The increase in both Young's modulus and maximum stress of SPM-**2**, along with increased deformation rate from 50 to 1,000 mm/min (Figure 2d), indicated the dynamic characteristics of quadruple H-bonding. Similar phenomena were also observed for ionically- and host/guest-crosslinked hydrogel networks.[32,33] The fracture strain of our material didn't change at low deformation rate (50 and 100 mm/min). At higher rates (≥200 mm/min), the strain-at-break decreased gradually (Figure 2d). To our surprise, the specimen of SPM-**2** can still be stretched up to 52x its original length with a maximum stress of 2.92 MPa at a high deformation rate of 1,000 mm/min (Movie 1 in Supporting Information (SI)). This ability to maintain high stretchability at high deformation rates is only observed with a few hydrogels[33] and rarely for other materials. These findings indicate the UPy H-bonding unit in SPM-**2** is able to undergo rapid exchange and reformation after dissociation under strain.

Our SPMs are also observed to dissipate mechanical energy during strain, as revealed by the large hysteresis in the cyclic stress-strain tests (Figure 2e). Even though only a 30% tensile strain is applied on the toughest sample (SPM-**3**), the hysteresis is still significant (Figure S15c). As shown in Figure S15d, a significant decrease of tensional stresses (by ~9.0%) in the second cycle was recorded if the film was stretched and released in two consecutive cycles. However, after a resting period of 1h, the film almost recovered its initial stress-strain behaviors, as seen by an overlap of the cyclic curves. These observations suggest that mechanical strain-caused dissociation of UPy crosslinks as a mechanism for strain energy dissipation.

Next, we performed crack propagation experiments on single-edged notched samples. Using SPM-**3** as an example, the notch area became blunt and was stable up to an average elongation of ~12× (Figure 2f and Movie 2 in SI). We observed that a crack initiated at the front of the notch, and then propagated quickly to break apart the specimen under continuous strain. Based on the large-strain approximation of Greensmith (Supplementary Equation 1),[34] we calculated the fracture energies of SPMs **1–3** to be 7,798, 30,888, 35,596 J/m^2, respectively (Figure 2g). In comparison, natural rubber[35a] and a multi-strength H-bonding elastomer based on PDMS matrix reported previously by our group[35b] have fracture energies of 10,000 and 12,000 J/m^2, respectively. The value

of the toughest hydrogel[22] based on ionically and covalently crosslinked network was 9,000 J/m^2, along with other well-known polymeric elastomers and hydrogels with noncovalent and covalent double networks possessing fracture energies in the range of 2,000 to 5,000 J/m^2 (Figure S16).[32,33,36] The high fracture energy for the SPMs is interesting, considering that the polymeric network is purely crosslinked by quadruple H-bonding. We attribute the observed high toughness to the prevalence of intramolecular and intermolecular loops from the strong UPy H-bonding dimerization and its high thermodynamic stability and rapid kinetic reversibility.

On account of dynamic bond and soft PTMG segment used in the materials design and preparation, we expect that the reversible UPy H-bonding (k_{off} = ~8 s^{-1})[26,27] would likely confer the SPMs with self-healing capability at room temperature. As observed by optical microscopy, the scratches on the SPM-**2** film almost totally disappeared after 12h healing at room temperature (Figure 2h), suggesting autonomous self-healing behavior. Subsequently, we cut the polymer specimen into two pieces with a scissor and put them back into contact for different self-healing periods under ambient conditions. Upon increasing the healing time, higher healing efficiencies were observed based on recovered fracture strain ratio which is defined as the ratio of fracture strain after healing divided by that before cutting (Figure 2i). For example, the healing efficiency was 12% after 6h and went up to 88% after 48h, along with a large fracture strain of ~15,000%. SPM-**1** reached almost quantitative healing efficiency while the self-healing efficiency of SPM-**3** was only 45% after healing 48h (Figure S17). This observed 'weakening' trend of the self-healing efficiency is attributed to the gradual increase in mechanical strength from SMP-**1** to SPM-**3**, as the availability of H-bonding as 'molecular glues' for self-healing are decreased. Factoring in mechanical properties, SPM-**2** showed a good balance of high fracture toughness and fast self-healing. Notably, the stress-strain curves of the self-healed SPM-**2** samples overlapped well with the original sample (Figure 2i), indicating good recovery of the mechanical properties after healing.

Stretchable and notch-insensitive thin-film gold electrodes. Using our new materials, stretchable thin-film gold electrodes are subsequently fabricated (see detailed fabrication procedures in SI). No additional treatments were needed to the polymeric substrate prior to thin gold film deposition. Interestingly, upon applying a tensile strain, the film was still conductive even at ~400% strain, a value which is much larger than that deposited on other commonly used polymer substrates, e.g. PDMS and polyurethane (PU) on which the gold film becomes non-conductive typically at 150% and 120% strain, respectively (Figure 3a). This may be attributed to the molecular design of our

polymers which include polar TEG groups. Aside from stretchability, notch-insensitive property is also useful for practical application of stretchable thin-film electrodes. For example, notches and defects are frequently found in thin-film electrodes either due to the repeated manipulations or by, for example, suturing during an operation. Therefore, we cut notches to the stretchable thin-film electrodes to check whether they can still maintain both conductivity and stretchability. Indeed, the film remained conductive even after inducing notches to the film (Figure 3b) and subsequently loading a tensile strain of ~260% (Figure 3d and Movie 3 in SI). Furthermore, we observed that our fabricated film did not break even after it was subjected to a ~ 300% tensile strain and then being partially cut with a scissor (Movie 4 in SI). As a comparison, a stretchable thin-film gold electrode on a PDMS substrate breaks into two parts at only ~40% applied strain (Figures 3b and e), even though the induced notch is shorter (Movie 5 in SI).

When a notch is introduced, the strain is more concentrated at the tip of the notch than the two ends of the film (Figure 3c). This will more likely result in crack propagation from the tip of the notch both in the polymeric substrate and in the metal thin film deposited on top, resulting in the electrode losing its conductivity. However, our supramolecular polymer-based stretchable gold thin-film electrodes with induced notches are still conductive when large tensile strains are applied, indicating that the electrode overcame the crack propagation both in the polymeric substrate and in the metal thin film. As a comparison, metal thin films are usually highly sensitive to the notch/defects during stretching, and throughout-cracks form readily for PDMS or PU substrate due to crack propagation (Figure S18). It is unusual that the induced cracks did not propagate from the notch tip throughout the metal film on our polymer. First, the mechanism of the stretchability of our gold film was investigated. We observed that at initial state even without any strain applied, the gold thin film already possessed initial randomly-distributed nano-cracks (Figure S19). They were formed due to the mismatch in thermal expansion coefficient between gold and the elastic substrate. The radiation heat during gold deposition causes greater thermal expansion of the elastomer and therefore generates nano-cracks as reported previously for other elastomers.[12] Under strain, the nano-cracks further developed into inter-connected micro-islands of randomly-distributed fractures. However, a conductive percolating network remained (Figures 3f–h). Such a morphology has previously been reported for gold thin-film electrodes[11,37,38], but the notch-insensitive property was not observed. The numerous micro-fractures have previously been shown as a mechanism for preventing the further propagation of the cracks under the strain. The applied strain energy to the gold film was assumed to be released by forming many micro fractures, instead of large cracks as

shown in Figure S18. In the case of our notch-tolerant substrate, since there is no tear of the substrate near the notch even at large strain, the notch only resulted in higher density of micro fractures near the notch, allowing the film to remain conductive through the network (Figures 3f–h). Thus, the high stretchability and notch-insensitivity of our SPM allowed stretchable and notch-insensitive gold thin-film electrodes to be achieved.

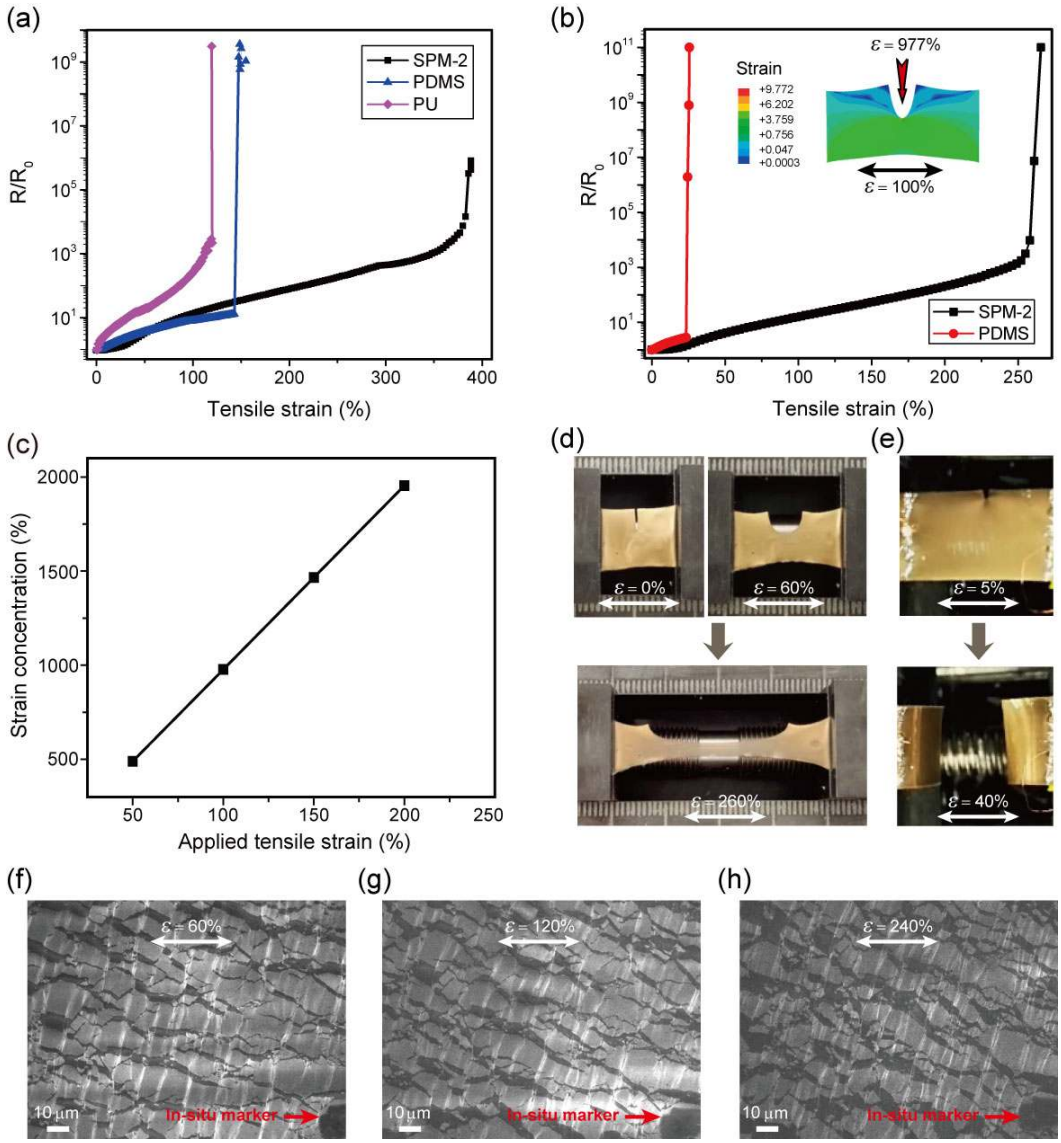

Figure 3. Highly stretchable thin film gold electrode with notch-insensitive property. (a) Stretchability comparison of the stretchable thin-film gold electrode on different polymeric substrates. The thickness of the gold film deposition is 50 nm with the same deposition condition. The conductor is taken as breaking when the normalized resistance increases sharply to around 10^9 Ω. (b) Stretchability comparison of the notched SPM-**2** electrode and PDMS electrode. Inset is the mechanical simulation by FEM to show the strain magnification effect induced by the notch. (c) Strain concentration at the tip of the notch calculated by FEM modeling. The strain concentration induced by the notch is much larger than the actual tensile strain applied. (d) Optical images to illustrate the stretching state of SPM-**2** based stretchable thin-film gold electrode with notch, and as

the comparison, the PDMS-based one is shown in (e). (**f**–**h**) In-situ SEM images to reveal the mechanism of SPM-**2** stretchable thin-film gold electrode. The randomly-distributed micro fractures assist the film to form a mesh structure under large mechanical deformation keeping the conductive path. The marker at lower right corner indicates the same position.

Self-healable stretchable thin-film electrodes. Besides the high stretchability and notch insensitivity, we also observed self-healing ability of the thin-film gold electrode deposited on SPM-**2** substrate. We note that previously reported self-healing electrodes were mostly based on liquid metal[35b] or composite materials.[13,39,40] In those systems, the conductive element was either a layer of liquid or conducting fillers dispersed in the thick self-healable polymer matrix. The conductive elements can easily re-contact each other to recover conductivity. However, for stretchable thin-film electrodes with the gold film of tens of nanometers in thickness, it is challenging to reconnect the gold film because their thicknesses are usually on the order of sub-micrometer. Here, a sharp blade was used to cut the electrode, with the gold thin film on the surface, into two halves and subsequently jointed back together by hand, i.e. no special alignment machine was used in this process (Figures 4a and S20). After allowing the electrode to heal for 36h at room temperature or 10h at 45 °C, the cut trace visibly remains but the conductivity of the gold film was recovered quantitatively (Figures 4a and b). Interestingly, we also observed that after the self-healing process of the polymeric substrate, the film was conductive even under 90% tensile strain (Figure 4b). We hypothesized that the mechanical deformation at the cutting edge induced by the blade played a key role for the stretchability. When the blade severed the electrode, we observed that the polymer adjacent to the cutting edge suffered plastic deformation and bend downwards, which was also verified by the finite element modeling (FEM) (Figures 4c-e). Bending of the polymer's edge was estimated to be ~50 micrometers by optical microscopy (Figure 4f), and the metal film was also covering the bent substrate surface (Figure 4g). Therefore, the gold film electrodes were able to reconnect, and thus re-establishing connectivity, as the side walls of the substrates became in contact to begin to heal (Figure 4h).

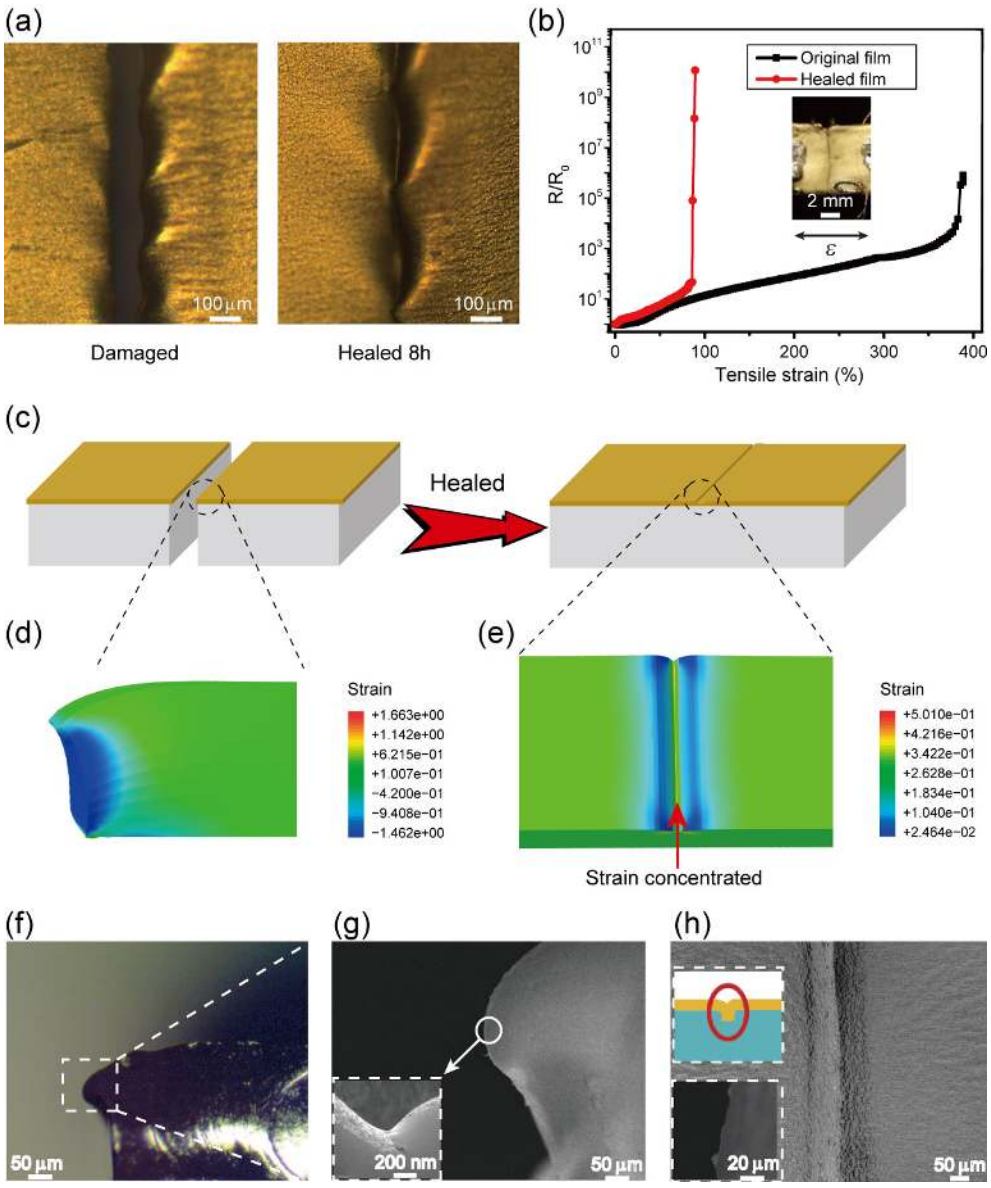

Figure 4. Self-healing property of the stretchable thin-film gold electrode. (a) Optical microscope images of the cut gold films before and after healed. It can be observed that the edge of the cut film keeps recurved even after healed. (b) Resistance change versus tensile strain to show the stretchability of the healed stretchable thin-film gold electrode. (c) Illustration images to show the before and after healed state of the film and the related mechanical simulation of the polymeric substrate by FEM is demonstrated in cross-section view in (d) to mechanically show the bending process at the cutting edge, and in top view in (e) to illustrate the strain distribution after healing under 25% tensile strain. More strain is concentrated at the scar decreasing the stretchability of the metal film. (f) Optical image of the cross-section of the cut gold film and polymeric substrate. (g) SEM image of the same sample in (f). The inset shows the magnified SEM image. (h) SEM image of the top view of the healed electrode. The upper inset shows the cartoon model of the healed electrode and the bottom inset displays the cross-section of the healed electrode.

On-skin and intramuscular EMG detection. Interfacial adhesion between the metal film and polymeric substrate is important as it was previously reported that a bad interfacial adhesion significantly affected the performance of the electrode, e.g. interface friction may cause delamination.[12] Thus, we investigated the interfacial adhesion of the thin-film metal electrode to various polymer substrates (Figure S21 and Movies 6–8 in SI). We observed the adhesion of the gold film was strong enough to pulled out the SPM-**2** polymer underneath to cause cohesive failure (Figure 5a shows the back side of the gold film can be observed through the transparent residual polymer), indicating very strong bonding between gold and SPM-**2**. Next, we compared the adhesion strength with two types of gold films on PDMS, i.e. with and without a 3 nm chromium as the adhesive layer. Interestingly, the adhesion strength of gold film on SPM-**2** is measured 3-4x higher than that of the other two (Figure 5b). The good adhesion is also important for reducing crack propagation in gold film as shown in other reports.[41]

Last, we proceed to demonstrate two potential applications of the stretchable gold electrodes as in-vitro and in-vivo electrophysiological sensors. First, for in-vitro measurements, we can reliably monitor electromyography signals (EMG) (Figures 5c and d). Electrodes were attached to the skin surface of the muscle by medical tapes and due to the good conformability of our soft electrodes, no adhesion gel was required to enhance the conformability. The obtained on-skin EMG signal is clean and signal-to-noise ratio is comparable to PDMS-supported gold electrodes (Figures 5d and e).[12,38] Second, for in-vivo measurements, we implanted the electrode into a rat to monitor the intramuscular myoelectric signal (Figures 5f and S22a). Briefly, the electrode was able to be sutured to the muscle to fix the detection position during the surgery (Figures S22b and S23). The signals obtained were both clear and stable (Figures 5g and h). So, here, we successfully demonstrated the potential of our novel stretchable thin-film electrode for both in-vitro and in-vivo measurements.

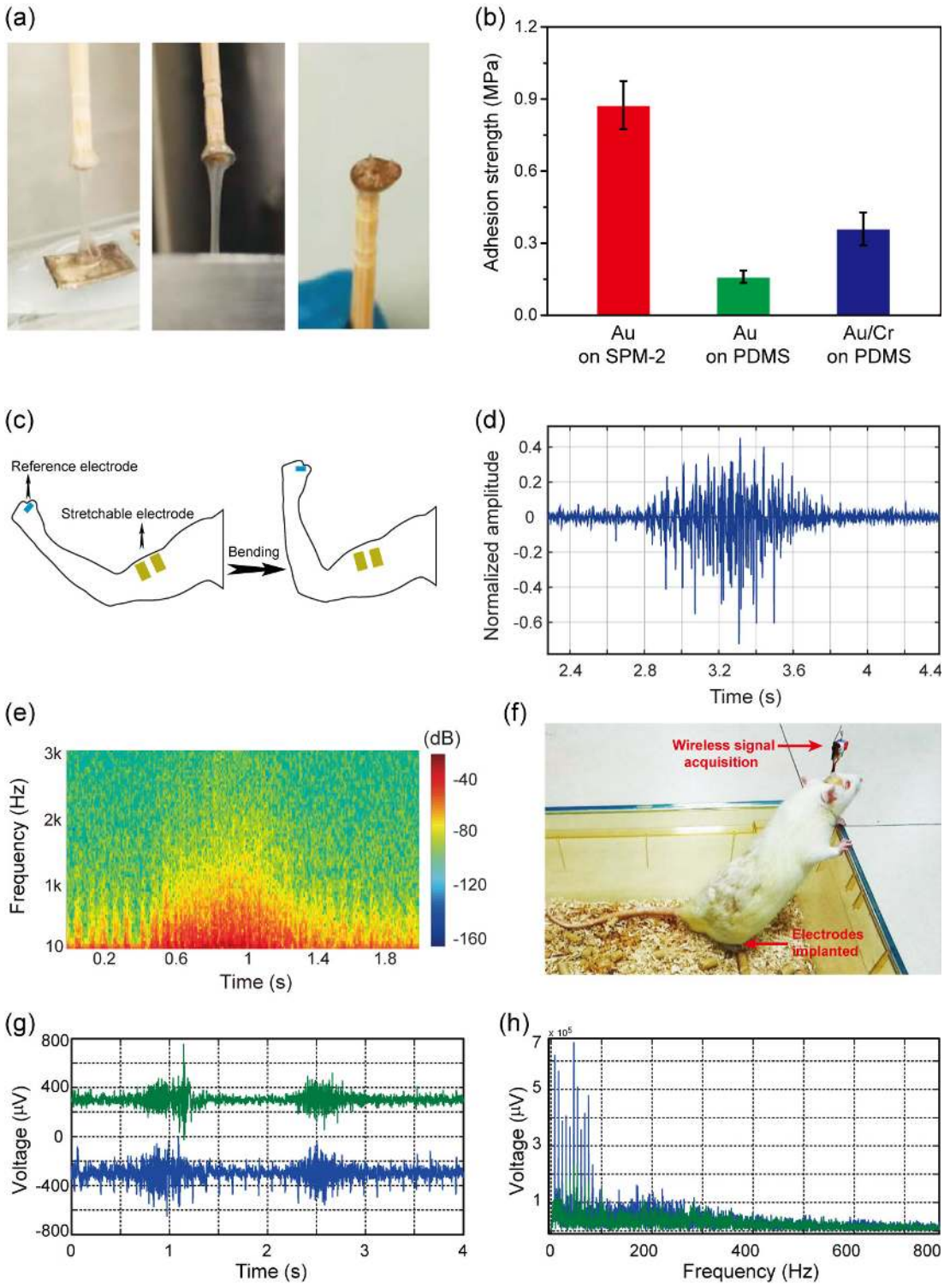

Figure 5. High-adhesion property of the electrode, and on-skin and in-vivo EMG detection. (a) Optical images of the adhesion testing process. The SPM-**2** is stretched out from the electrode indicating that the adhesion between the gold film and SPM-**2** is quite good, and the adhesion strength is determined by the polymer substrate itself not by the interfacial adhesion between the gold film and the polymer. The right panel shows the final state at the bottom of the stick. The residual breaking polymer can be observed clearly and the yellow gold film is underneath. (b) Adhesion strength of SPM-**2** based electrode compared with the one based on PDMS and non-

stretchable electrode. (c) Sketch of the on-skin EMG detection. Two yellow parts illustrate the electrode position and the blue part shows the reference electrode. (d) Typical EMG signal detected. (e) Energy spectrum analysis of the EMG signal in (d). (f) Side view of the rat implanted with SPM-**2** based stretchable thin-film gold electrode. See details of implanted process and electrode position in Figure S22. (g) Typical subcutaneous EMG signal. (h) Spectrum analysis of the EMG signal in (g).

CONCLUSION

In summary, we have described a molecular design approach to achieve stretchable, anti-tearing, and self-healing metal thin-film electrodes. Our presented results indicated the functionalities of stretchable thin-film electrodes can be significantly enhanced through the chemical design of the polymeric substrate. In specific, we applied supramolecular polymer design principles to synthesize dynamically crosslinked SPMs via quadruple UPy H-bonding. The resulting SPM contained multiple intra- and inter-chain H-bonding in the polymeric networks to enable excellent mechanical properties. Subsequently, our fabricated thin film gold electrode from the SPM substrate possesses both excellent inherent conductivity and unique mechanical behaviors. Our electrodes have many of the highly desirable parameters combined into a single thin-film electrode, which include high stretchability, self-healing, notch insensitivity and improved interfacial adhesion. Finally, this stretchable electrode was successfully shown to measure EMG signals both on human skin (in-vitro) and implanted within live rats (in-vivo). These demonstrations clearly indicate that our SPM-supported thin film gold electrodes are potentially promising toward the fabrication of next-generation wearable and implantable electronics.

ASSOCIATED CONTEN

Supporting Information

Experimental details and additional data. This material is available free of charge via the Internet at http://pubs.acs.org.

AUTHOR INFORMATION

Corresponding Authors

*chenxd@ntu.edu.sg (X.C.)

*zbao@stanford.edu (Z.B.)

ORCID

Xuzhou Yan: 0000-0002-6114-5743

Qiuhong Zhang: 0000-0001-5699-2270

Jeffrey Lopez: 0000-0002-6425-5550

Hung-Chin Wu: 0000-0001-6492-0525

Ting Lei: 0000-0001-8190-9483

Xiaodong Chen: 0000-0002-3312-1664

Zhenan Bao: 0000-0002-0972-1715

Author Contributions

[#]These authors contributed equally to this work.

Notes

The authors declare no competing financial interest.

ACKNOWLEDGEMENTS

Z.B. acknowledges support from Air Force Office of Scientific Research (grant No. FA9550-15-1-0106). X.C. thanks the financial support from the National Research Foundation, Prime Minister's Office, Singapore under its NRF Investigatorship (NRF2016NRF-NRFI001-21) and Singapore Ministry of Education (MOE2015-T2-2-060). Q.Z. thanks the financial support from National Natural Science Foundation of China (21404056) and China Scholarship Council (201606195042). G.L. thanks the support from the National Natural Science Foundation of China under grants (#U1613222). J.L. acknowledges support by the National Science Foundation Graduate Research Fellowship Program (grant No. DGE-114747). Part of this work was performed at the Stanford Nano Shared Facilities (SNSF), supported by the National Science Foundation under award ECCS-1542152. Use of the Stanford Synchrotron Radiation Lightsource, SLAC National Accelerator Laboratory, is supported by the U.S. Department of Energy, Office of Science, Office of Basic Energy Sciences under Contract No. DE-AC02-76SF00515. The SSRL Structural Molecular Biology Program is supported by the DOE Office of Biological and Environmental Research, and by the National Institutes of Health, National Institute of General Medical Sciences (including P41GM103393). The contents of this publication are solely the responsibility of the authors and do not necessarily represent the official views of NIGMS or NIH. We thank Ivan Rajkovic for the support at Beamline 4-2.

REFERENCES

1. Chen, D.; Pei, Q. *Chem. Rev.* **2017**, *117*, 11239–11268.
2. Someya, T.; Bao, Z.; Malliaras, G. G. *Nature* **2016**, *540*, 379–385.
3. Xu, S.; Zhang, Y.; Jia, L.; Mathewson, K. E.; Jang, K.-I.; Kim, J.; Fu, H.; Huang, X.; Chava, P.; Wang, R.; Bhole, S.; Wang, L.; Na, Y. J.; Guan, Y.; Flavin, M.; Han, Z.; Huang, Y.; Rogers, J. A. *Science* **2014**, *334*, 70–74.
4. Chortos, A.; Liu, J.; Bao, Z. *Nature Mater.* **2016**, *15*, 937–950.
5. Liu, J.; Fu, T.-M.; Cheng, Z.; Hong, G.; Zhou, T.; Jin, L.; Duvvuri, M.; Jiang, Z.; Kruskal, P.; Xie, C.; Suo, Z.; Fang, Y. Lieber, C. M. *Nature Nanotech.* **2015**, *10*, 629–636.
6. Li, J.; Ávila, B. E.-F. de; Gao, W.; Zhang, L.; Wang, J. *Sci. Robot.* **2017**, *2*, eaam6431.
7. Xiao, J.; Carlson, A.; Liu, Z. J.; Huang, Y.; Jiang, H.; Rogers, J. A. *Appl. Phys. Lett.* **2008**, *93*, 013109.
8. Yeo, W. H.; Kim, Y.-S.; Lee, J.; Ameen, A.; Shi, L.; Li, M.; Wang, S.; Ma, R.; Jin, S. H.; Kang, Z.; Huang, Y.; Rogers, J. A. *Adv. Mater.* **2013**, *25*, 2773–2778.
9. Liang, J.; Li, L.; Tong, K.; Ren, Z.; Hu, W.; Niu, X.; Chen, Y.; Pei, Q. *ACS Nano* **2014**, *8*, 1590−1600.
10. Guo, C. F.; Sun, T.; Liu, Q.; Suo, Z.; Ren, Z. *Nature Commun.* **2014**, *5*, 3121.
11. Lacour, S. P.; Chan, D.; Wagner, S.; Li, T.; Suo, Z. *Appl. Phys. Lett.* **2006**, *88*, 204103.
12. Liu, Z.; Wang, X.; Qi, D.; Xu, C.; Yu, J.; Liu, Y.; Jiang, Y.; Liedberg, B.; Chen, X. *Adv. Mater.* **2017**, *29*, 1603382.
13. (a) Tee, B. C.-K.; Wang, C.; Allen, R.; Bao, Z. *Nature Nanotech.* **2012**, *7*, 825–832. (b) Gong, C.; Liang, J.; Hu, W.; Niu, X.; Ma, S.; Hahn, T.; Pei, Q. *Adv. Mater.* **2013**, *25*, 4186–4191.
14. (a) Huynh, T.-P.; Haick, H. *Adv. Mater.* **2016**, *28*, 138–143. (b) Ko, J.; Kim, Y.-J.; Kim, Y. S. *ACS Appl. Mater. Interfaces* **2016**, *8*, 23854–23861.
15. (a) Blaiszik, B. J.; Kramer, S. L. B.; Crady, M. E.; Mcllroy, D. A.; Moore, J. S.; Sottos, N. R.; White, S. R. *Adv. Mater.* **2012**, *24*, 398–401. (b) Cai, G.; Wang, J.; Qian, K.; Chen, J.; Li, S.; Lee, P. S. *Adv. Mater.* **2017**, *4*, 1600190. (c) Kim, K.; Jung, M.; Kim, B.; Kim, J.; Shin, K.; Kwon, O.-S.; Jeon, S. *Nano Energy* **2017**, *41*, 301–307. (c) Kim, S.-M.; Jeon, H.; Shin, S.-H.; Park, S.-A.; Jegal, J.; Hwang, S. Y.; Oh, D. X.; Park, J. *Adv. Mater.* **2018**, *30*, 1705145.
16. Chen, X. *Small Methods* **2017**, *1*, 1600029.
17. Aida, T.; Meijer, E. W.; Stupp, S. I. *Science* **2012**, *335*, 813–817.
18. Greef, T. F. A. De; Smulders, M. M. J.; Wolffs, M.; Schenning, A. P. H. J.; Sijbesma, R. P.; Meijer, E. W. *Chem. Rev.* 2009, *109*, 5687–5754.

19. Yang, L.; Tan, X.; Wang, Z.; Zhang, X. *Chem. Rev.* **2015**, *115*, 7196–7239.
20. Yan, X.; Wang, F.; Zheng, B.; Huang, F. *Chem. Soc. Rev.* **2012**, *41*, 6042–6065.
21. Wojtecki, R. J.; Meador, M. A.; Rowan, S. J. *Nature Mater.* **2011**, *10*, 14–27.
22. Sun, J.-Y. Zhao, X.; Illeperuma, W. R. K.; Chaudhuri, O.; Oh, K. H.; Mooney, D. J.; Vlassak, J. J.; Suo, Z. *Nature* **2012**, *489*, 133–136.
23. Kushner, A. M.; Vossler, J. D.; Williams, G. A.; Guan, Z. *J. Am. Chem. Soc.* **2009**, *131*, 8766–8768.
24. Guan, Z.; Roland, J. T.; Bai, J. Z.; Ma, S. X.; Mclntire, T. M.; Nguyen, M. *J. Am. Chem. Soc.* **2004**, *126*, 2058–2065.
25. Li, C.-H.; Wang, C.; Keplinger, C.; Zuo, J.-L.; Jin, L.; Sun, Y.; Zheng, P.; Cao, Y.; Lissel, F.; Linder, C.; You, X.-Z.; Bao, Z. *Nature Chem.* **2016**, *8*, 618–624.
26. Sijbesma, R. P.; Beijer, F. H.; Brunsveld, L.; Folmer, B. J. B.; Hirschberg, J. H. K. Ky; Lange, R. F. M.; Lowe, J. K. L.; Meijer, E. W. *Science* **1997**, *278*, 1601–1604.
27. Söntjens, S. H. M.; Sijbesma, R. P.; Genderen, M. H. P. van; Meijer, E. W. *J. Am. Chem. Soc.* **2000**, *122*, 7487–7493.
28. (a) Yan, X.; Li, S.; Pollock, J. B.; Cook, T. R.; Chen, J.; Zhang, Y.; Ji, X.; Yu, Y.; Huang, F.; Stang, P. J. *Proc. Natl. Acad. Sci. U.S.A.* **2013**, *110*, 15585–15590. (b) Qin, B.; Zhang, S.; Song, Q.; Huang, Z.; Xu, J.-F.; Zhang, X. *Angew. Chem. Int. Ed.* **2017**, *56*, 7639–7643.
29. Jeon, I.; Cui, J.; Illeperuma, W. R. K.; Aizenberg, J.; Vlassak, J. J. *Adv. Mater.* **2016**, *28*, 4678–4683.
30. Chen, Y.; Kushner, A. M.; Williams, G. A.; Guan, Z. *Nature Chem.* **2012**, *4*, 467–472.
31. Sun, G.; Li, Z.; Liang, R.; Weng, L.-T.; Zhang, L. *Nature Commun.* **2016**, *7*, 12095.
32. Sun, T. L.; Kurokawa, T.; Kuroda, S.; Ihsan, A. B.; Akasaki, T.; Sato, K.; Haque, M. A.; Nakajima, T.; Gong, J. P. *Nature Mater.* **2013**, *12*, 932–937.
33. Liu, J.; Tan, C. S. Y.; Yu, Z.; Lan, Y.; Abell, C.; Scherman, O. A. *Adv. Mater.* **2017**, *29*, 1604951.
34. Greensmith, H. W. *J. Appl. Polym. Sci.* **1963**, *7*, 993–1002.
35. (a) Sakulkaew, K.; Thomas, A. G.; Busfield, J. J. C. *Polym. Test.* **2011**, *30*, 163–172. (b) Kang, J.; Son, D.; Wang, G.-J. N.; Liu, Y.; Lopez, J.; Kim, Y.; Oh, J.-Y.; Katsumata, T.; Mun, J.; Lee, Y.; Jin, L.; Tok, J. B.-H.; Bao, Z. *Adv. Mater.* **2018**, *30*, 1706846.
36. Ducrot, E.; Chen, Y.; Bulter, M.; Sijbesma, R. P.; Creton, C. *Science* **2014,** *344*, 186–189.
37. Liu, Z.; Yu, M.; Lv, J.; Li, Y.; Yu, Z. *ACS Appl. Mater. & Interfaces* **2014**, *6*, 13487–13495.
38. Liu, Z.; Qi, D.; Guo, P.; Liu, Y.; Zhu, B.; Yang, H.; Liu, Y.; Li, B.; Zhang, C.; Yu, J.; Liedberg, B.; Chen, X. *Adv. Mater.* **2015**, *27*, 6230–6237.
39. Benight, S. J.; Wang, C.; Tok, J. B.-H.; Bao, Z. *Prog. Polym. Sci.* **2013**, *38*, 1961–1977.

40. Wang, H.; Zhu, B.; Jiang, W.; Yang, Y.; Leow, W. R.; Wang, H.; Chen, X. *Adv. Mater.* **2014**, *26*, 3638–3643.

41. (a) Bitter, J. E.; Lardner, T. J.; Grayeski, W.; Prakash, G. C.; Lawrence, J. *J. Adhes.* **1997**, *63*, 265–284. (b) Potter, K. D.; Guild, F. J.; Harvey, H. J.; Wisnom, M. R.; Adams, R. D. *Int. J. Adhes. Adhes.* **2001**, *21*, 435–443. (c) Suo, Z.; Vlassak, J.; Wagner, S. *China Particuology* **2005**, *3*, 321–328.

TOC Graphic